

# Joint scientific session of the Physical Sciences Division of the Russian Academy of Sciences and the Joint Physical Society of the Russian Federation (honoring the 110th birthday of P L Kapitza and the 70th anniversary of the P L Kapitza Institute for Physical Problems) (16 June 2004)

On 16 June 2004, a joint scientific session of the Physical Sciences Division of the Russian Academy of Sciences and the Joint Physical Society of the Russian Federation was held in the Conference Hall of the P L Kapitza Institute for Physical Problems, Russian Academy of Sciences, to honor the 110th birthday of P L Kapitza and the 70th anniversary of the host institute. The following reports were presented at the session:

(1) **Andreev A F** (P L Kapitza Institute for Physical Problems, RAS, Moscow) “Quantum crystals”;

(2) **Dmitriev V V** (P L Kapitza Institute for Physical Problems, RAS, Moscow) “Spin superfluidity in  $^3\text{He}$ ”;

(3) **Lebedev V V** (L D Landau Institute of Solid State Physics, RAS, Chernogolovka, Moscow Region) “Theory of weak crystallization”;

(4) **Sosin S S, Prozorova L A, Smirnov A I** (P L Kapitza Institute for Physical Problems, RAS, Moscow) “New magnetic states in crystals”.

Abridged versions of reports 2 and 4 are given below.

PACS numbers: 67.57.–z, 67.57.Lm

DOI: 10.1070/PU2005v048n01ABEH001904

## Spin superfluidity in $^3\text{He}$

V V Dmitriev

### 1. Introduction

The hallmark of a superfluid liquid is its ability to assume quantum coherence, a state with a special kind of long-range order. The key characteristic describing this order in superfluid  $^4\text{He}$  or common superconductors is a complex wave function, the so-called condensate wave function  $\Psi = |\Psi| \exp(i\varphi)$  with a definite phase  $\varphi$ . This implies that the gauge invariance of the system breaks down at the superfluid transition. While the energy of superfluid liquid does not depend on the phase, it increases if  $\varphi$  becomes spatially nonuniform (i.e., when the so-called order parameter gradient energy increases). This gives rise to the mass- and (in superconductors) charge-carrying superfluid current

$$J_S = \frac{\hbar}{m} |\Psi|^2 \nabla \varphi = \rho_S v_S, \quad (1)$$

where  $m$  is the mass of the  $^4\text{He}$  atom and  $\rho_S = |\Psi|^2$  and  $v_S = (\hbar/m) \nabla \varphi$  are the superfluid component density and velocity, respectively. A constant phase difference  $\Delta\varphi$  maintained between the ends of a channel filled with superfluid  $^4\text{He}$  will give rise to a nondissipative current through the channel, whose magnitude will be proportional to this phase difference rather than the pressure or chemical potential difference as in a normal liquid. Correspondingly, electrical current in a superconductor is determined by the wave function phase difference between the electrons at the ends of the sample rather than by the voltage, as in a common conductor. The gradient energy can be viewed as kinetic energy associated with the superfluid current,  $F_V = \rho_S v_S^2/2$ , and the current is correspondingly written as  $J_S = \partial F_V / \partial v_S$ .

Unlike the atoms of  $^4\text{He}$ , the atoms of  $^3\text{He}$  are fermions, implying that their superfluidity results from Cooper pairing (analogous to superconductivity in metals). What is essentially new compared to common superconductors is that the spin and orbital moments of  $^3\text{He}$  Cooper pairs are 1. Accordingly, there are three possible values for the projection of both the spin and the orbital moment on a chosen direction, and the order parameter is conveniently taken in the form of a complex  $3 \times 3$  matrix which describes, in particular, how the spin and orbital moments of a Cooper pair are oriented with respect to one another (for more details on superfluid  $^3\text{He}$ , see Refs [1–3]). Such ordering may correspond to various superfluid phases differing in the specific form of this matrix. In superfluid  $^3\text{He}$ , only three phases —  $^3\text{He-A}$ ,  $^3\text{He-A}_1$ , and  $^3\text{He-B}$  — are found, depending on conditions (Fig. 1). In these phases, symmetries other than the gauge symmetry can also be violated. In particular, the violation of spin rotation symmetry in Cooper pairs leads to three additional hydrodynamic variables similar to the order parameter phase. The gradients of these variables will give rise to a spin supercurrent, a current in which spin and the related magnetic moment are transferred in a non-dissipative way (we do not distinguish between spin and magnetic currents below). It should be noted that what is meant by a spin supercurrent is magnetization transferred in the absence of mass transfer, not the flow of magnetized material. In general, the spin supercurrent is a tensor and can be written as

$$J_{kv} = \frac{\hbar}{2m} \rho_{ikv\sigma} \Omega_{i\sigma}, \quad (2)$$

where  $\rho_{ikv\sigma}$ , the tensor of the superfluid spin density, is on the order of  $\chi c^2/g$ ;  $c$  is a factor in the expression for the gradient energy and has the meaning of spin wave velocity;  $\chi$  is the

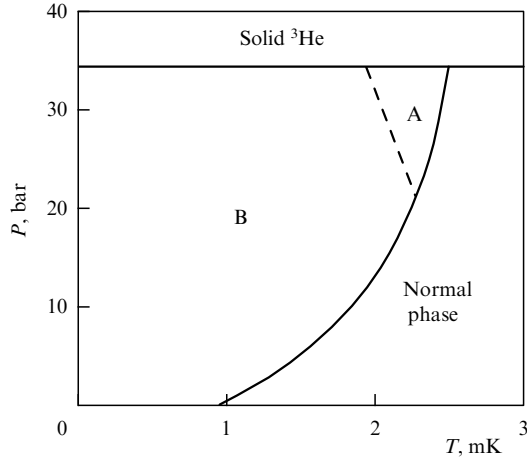


**Figure 1.** Phase diagram of  $^3\text{He}$  in zero magnetic field. The  $A_1$ -phase occurs only in a magnetic field in a narrow region around the superfluid transition temperature.

magnetic susceptibility;  $g$  the gyromagnetic ratio; and  $\Omega_{i\sigma}$  is a tensor characterizing the non-uniformity in spin space orientation.  $i$  and  $k$  are coordinate space indices, and  $\nu$  and  $\sigma$  are spin space indices.

The following reasoning leads to a simple model of how a spin supercurrent appears. In the momentum representation the wave function of a spin-1 Cooper pair can be expanded in components corresponding to various values of the projection of the Cooper pair spin ( $m_s = 1, 0, -1$ ) onto a chosen direction, giving

$$\Psi = \Psi_{\uparrow\uparrow}|1, 1\rangle + \Psi_{\downarrow\downarrow}|1, -1\rangle + \frac{1}{\sqrt{2}}(\Psi_{\uparrow\downarrow} + \Psi_{\downarrow\uparrow})|1, 0\rangle, \quad (3)$$

where the  $|1, m_s\rangle$  are the eigenfunctions of the spin operator projection. Now consider superfluid  $^3\text{He}$  as consisting of a normal component and three superfluid components with wave functions  $\Psi_{\uparrow\uparrow}$ ,  $\Psi_{\downarrow\downarrow}$ , and  $(\Psi_{\uparrow\downarrow} + \Psi_{\downarrow\uparrow})$ . Because in weak magnetic fields  $|\Psi_{\uparrow\uparrow}| = |\Psi_{\downarrow\downarrow}|$ , the counterflow of  $\Psi_{\uparrow\uparrow}$  and  $\Psi_{\downarrow\downarrow}$  should lead to superfluid spin transfer in the absence of mass transfer.

The possibility of a spin supercurrent began to be widely discussed immediately after the 1972 discovery of superfluidity in  $^3\text{He}$  [4], when it became clear that the Cooper pairs of the new superfluid phases have a spin. However, direct evidence for the existence of such currents was lacking for a long time, leaving it unclear precisely which of the observable phenomena are caused by spin supercurrents and under what conditions these phenomena can be observed. The experiments A S Borovik-Romanov and his team started at the P L Kapitza Institute for Physical Problems in 1984 and theoretical work by I A Fomin of the L D Landau Institute of Theoretical Physics provided elucidation of the problem. In the present paper, a brief review of these studies is given. The experiments described in Section 4–7 were conducted at pressures from 0 to 29.3 bar in magnetic fields from 71 to 570 Oe [the corresponding nuclear magnetic resonance (NMR) frequencies ranging from 230 kHz to 1.85 MHz]. The problem of magnetic superfluidity can also be found in the review papers [5–8].

## 2. Spin supercurrent in $^3\text{He-B}$

The violation of the spin space rotation symmetry in superfluid  $^3\text{He}$  does not yet mean that spin supercurrent is easy to

create and measure there. Unlike mass or electric charge, spin is not generally a conserved quantity. For example, the spin-orbit (dipole) interaction can lead to spin transfer to other degrees of freedom, and spin supercurrents can be considered meaningfully only if their effect is noticeable compared to spin-non-conserving processes. In superfluid  $^3\text{He}$  spin-orbit interaction can be important because it is stronger than in the normal phase (due to the fact that Cooper pairs have a spin and an orbital moment). For this reason, talking about spin supercurrents only makes sense with respect to the B-phase, in which the spin-orbit interaction can be effectively eliminated. Therefore, the discussion below is limited to the B-phase.

The order parameter of the B-phase has the form

$$A_{vi} = \Delta \exp(i\varphi) \hat{R}_{vi}(\hat{\mathbf{n}}, \theta) = \Delta \exp(i\varphi) \hat{R}_{vi}(\alpha, \beta, \gamma), \quad (4)$$

where  $\Delta$  is the energy gap in the excitation spectrum and  $\varphi$  is the phase of the orbital part of the order parameter (a gradient of  $\varphi$  produces a mass supercurrent). The matrix  $\hat{R}(\hat{\mathbf{n}}, \theta)$  of size  $3 \times 3$  rotates the spin space with respect to the orbital space through an angle  $\theta$  about the direction  $\hat{\mathbf{n}}$  (which is common for a macroscopic volume of  $^3\text{He}$ ). Another way to express this rotation is in terms of the Euler angles  $\alpha$ ,  $\beta$ , and  $\gamma$ . The angle  $\theta$  can in principle take on any value. In equilibrium, this degeneracy is lifted by imposing a minimum condition on the dipole energy

$$F_D = \frac{8}{15} \frac{\chi}{g^2} \Omega_B^2 \left( \frac{1}{4} + \cos \theta \right)^2, \quad (5)$$

where  $\Omega_B = \Omega_B(T)$ , the so-called Leggett frequency, is a temperature-dependent characteristic of the dipole interaction force [ $\Omega_B(0) \sim 200$  kHz]. The minimum of the dipole energy is achieved at

$$\theta = \theta_0 = \arccos\left(-\frac{1}{4}\right) \approx 104^\circ.$$

To excite a spin supercurrent, NMR experiments can be used. In an NMR experiment the spin part of the order parameter is in motion, the angles  $\alpha$ ,  $\beta$ , and  $\gamma$  depend on time, and the first two of them have a simple physical meaning:  $\alpha$  corresponds to the phase of the magnetization precession, and  $\beta$  to the magnetization deviation angle from the equilibrium direction. The contributions due to the gradients of these angles lead to an increase in the spin gradient energy and hence produce a spin supercurrent.

In the spatially uniform case the spin dynamics of  $^3\text{He-B}$  is determined by the Leggett–Takagi equations [9, 10]

$$\begin{aligned} \dot{\mathbf{M}} &= g\mathbf{M} \times \mathbf{H} + \frac{4}{15} \frac{\chi \Omega_B^2}{g} \sin \theta (1 + 4 \cos \theta) \hat{\mathbf{n}}, \\ \dot{\theta} &= g\hat{\mathbf{n}} \cdot \left( \frac{\mathbf{M}}{\chi} - \mathbf{H} \right) + \frac{4}{15\tau} \sin \theta (1 + 4 \cos \theta), \\ \dot{\hat{\mathbf{n}}} &= -\frac{g}{2} \left\{ \hat{\mathbf{n}} \times \left( \frac{\mathbf{M}}{\chi} - \mathbf{H} \right) + \cot \frac{\theta}{2} \left[ \hat{\mathbf{n}} \times \left[ \hat{\mathbf{n}} \times \left( \frac{\mathbf{M}}{\chi} - \mathbf{H} \right) \right] \right] \right\}, \end{aligned} \quad (6)$$

where  $\tau$  is the Leggett–Takagi effective time determining the magnetic relaxation rate. There are a number of NMR modes (i.e., of periodic magnetization motions) that follow from Eqn (6), of which the easiest to excite is the so-called Brinkman–Smith mode [11], that is the precession of magnetization deviated by an angle  $\beta < \theta_0$  from the direction

of  $\mathbf{H}$  (with  $|\mathbf{M}| = \chi H$ ). What is remarkable about this mode is that  $\theta = \theta_0$ , i.e., the dipole energy remains zero during this precession. As a result, the last term on the right-hand side of the first equation of system (6) also goes to zero, as does the relaxation term in the second equation. Note that both the magnetization and the vector  $\hat{\mathbf{n}}$  precess at the Larmor frequency (the orientation of  $\hat{\mathbf{n}}$  relative to  $\mathbf{M}$  is determined by precisely the condition that the dipole energy be a minimum). Let the magnetic field  $\mathbf{H}$  be along the  $z$  axis and suppose that the system is homogeneous in the plane  $x, y$  but has inhomogeneities along the  $z$ -axis. Then, allowing for spin currents, the first equation of system (6) can be rewritten in the form

$$\dot{M}_v = (g\mathbf{M} \times \mathbf{H})_v + \frac{\partial J_{zv}}{\partial z}, \quad (7)$$

where  $v$  indexes the magnetization and current components ( $x, y$ , and  $z$ ). For  $M_z$ , the first term on the right-hand side of Eqn (7) is zero, thus yielding the magnetization equation of continuity. If we transform to a Larmor-frequency-rotating coordinate system, this equation is also fulfilled for  $M_x$  and  $M_y$ , which is exactly what enables effects related to the spin supercurrent to be observed.

Given the minimum condition for the dipole energy, two of the three Euler angles (for example,  $\alpha$  and  $\beta$ ) can be chosen as independent, and in terms of the gradients of these two it is possible to obtain formulas for the spin supercurrent [12, 13]. For example, the spin supercurrent carrying the  $z$ -component of the magnetization in the direction of the  $z$ -axis is found to be

$$J_{zz} = -\frac{\chi}{g} c^2 \sqrt{1-u} \left[ f_1(u) \frac{\partial \alpha}{\partial z} + f_2(u) \frac{\partial \beta}{\partial z} \right], \quad (8)$$

where  $u = \cos \beta$ ,

$$f_1(u) = (2+u)\sqrt{1-u}, \quad f_2(u) = \sqrt{\frac{3}{(1+4u)(1+u)}}.$$

From Eqn (8) it is seen that the analog of superfluid density in spin superfluidity is a quantity proportional to  $\sqrt{1-u}$ . Therefore, superfluid spin density is different from zero only for  $\beta \neq 0$ .

If the angle  $\beta > \theta_0$ , the dipole energy is minimum — but already not zero — at  $\theta = \beta$ , which results in a positive shift in the NMR frequency [11],

$$\omega - \omega_L = -\frac{4}{15} \frac{\Omega_B^2}{\omega_L} (1 + 4 \cos \beta), \quad (9)$$

where  $\omega$  and  $\omega_L = gH$  are the precession and Larmor frequencies, respectively. Note that the dipole moment on the right-hand side of the first equation of system (6) (and the relaxation term in the second) are also nonzero. Fortunately, under the conditions of the experiments to be described in Sections 3–7, these additional terms are small, and their associated non-conservation of spin affects spin dynamics little compared to magnetization transfer by spin currents.

### 3. A homogeneously precessing domain

There is an important consequence of the fact that  $^3\text{He-B}$  can carry a spin supercurrent: the formation of the so-called homogeneously precessing domain (HPD). Let us see how an HPD forms under pulsed NMR conditions (Fig. 2). Let a

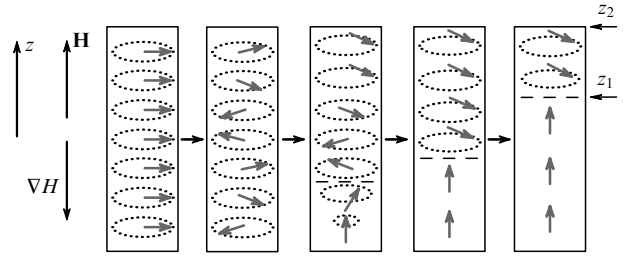


Figure 2. Formation of an HPD after the application of a deflecting rf pulse.

sample of  $^3\text{He-B}$  be placed in a closed cell and exposed to a uniform magnetic field gradient. At equilibrium the magnetization is parallel to the field. Now let us apply a short rf pulse to get the magnetization deflected through a certain angle ( $90^\circ$  in Fig. 2) throughout the volume. Then the magnetization in the volume enters the Brinkman–Smith mode, i.e., starts precessing at the Larmor frequency — which is coordinate dependent [ $\omega_L(z) = \omega_L(0) - zg\nabla H$ ] because the magnetic field varies along the cell — and the phase of the precession develops a gradient which increases with time. As the magnetization precesses, it produces an induction signal in the NMR pickup coil, for which, in a system of non-interacting spins, the decay time due to dephasing must be  $T_2^* \sim 1/\Delta\omega = 1/(gL\nabla H)$ , where  $\Delta\omega$  is the characteristic precession frequency range over the cell and  $L$  the cell length. A different picture arises for  $^3\text{He-B}$ . According to Eqn (8), a gradient in precession frequency leads to a spin supercurrent, which transports the longitudinal magnetization along the field gradient direction. Because there is no spin flow through the cell boundaries, the longitudinal component of the magnetization starts changing: the magnetic moment flows down to the bottom of the cell (here,  $M_z$  increases) and away from its top (here,  $M_z$  decreases). Since the absolute value of  $\mathbf{M}$  in the Brinkman–Smith mode cannot change — this would lead to an increase in the dipole energy — what the change in the longitudinal magnetization does is to cause a change in the deviation angle  $\beta$ , upwards at the top and downwards at the bottom of the cell. This can continue until  $0 < \beta < \theta_0$ . At  $\beta = 0$  we have the condition  $J_{zz} = 0$ , meaning that magnetization ceases to be transported in this region. As the angle  $\beta$  increases above  $\theta_0 \approx 104^\circ$ , the dipole energy increases, and the precession frequency shifts from the Larmor value [see Eqn (9)]. This frequency shift can in principle (and does in practice) compensate for the nonuniform field and turn  $\partial\alpha/\partial z$  and  $J_{zz}$  to zero. Accordingly, regions with  $J_{zz} = 0$  appear and grow at the ends of the cell (a  $\beta = 0$  region at the lower end and a  $\beta \geq \theta_0$  region at the upper end) to ultimately occupy the entire volume of the cell and form the so-called two-domain structure, where spin supercurrents are zero [13]. The lower domain is in fact unperturbed  $^3\text{He-B}$  (a static domain, SD), whereas in the upper so-called homogeneously precessing domain the magnetization deviates by slightly more than  $\theta_0$  and precesses. This angle excess  $\delta\beta = \beta - \theta_0$  depends on  $z$  in such a way that the resulting frequency shift compensates for the nonuniform field (nonuniform Larmor frequency) and the precession phase is the same throughout the sample, whereas the precession frequency is equal to the Larmor value  $\omega_L(z_1)$ , where  $z_1$  indicates the location of the interdomain wall. Under realistic experimental conditions ( $H \sim 100$  Oe,  $\nabla H_z \sim 1$  Oe  $\text{cm}^{-1}$ ,  $L \sim 0.5$  cm),  $\delta\beta \sim 1^\circ$ , and the produced

dipole moment is sufficiently small, suggesting that the dynamics of the magnetization remain to be largely determined by the spin supercurrents: nonuniformities in the HPD lead to currents which cause the system to precess uniformly as before.

The interdomain wall has a characteristic thickness  $\lambda = [c^2/(\omega\nabla\omega)]^{1/3} \sim 0.5$  mm. The angle  $\beta$  in the wall changes smoothly from  $\sim 104^\circ$  to zero. In addition, the angle  $\alpha$  changes by about  $60^\circ$ . Exactly how  $\alpha$  and  $\beta$  change is determined by two conditions: first, the spin current in the wall due to inhomogeneities in  $\beta$  is compensated by the current due to inhomogeneities in  $\alpha$ ; and second, the precession frequency in the wall equals that of the entire HPD (because  $\beta < \theta_0$  in the wall, the small frequency shift which is needed is ensured by the gradient energy [13]).

Magnetic relaxation in the two-domain structure proceeds by spin diffusion in the interdomain wall and by the Leggett–Takagi mechanism [10] in the bulk of the HPD, where there is a small shift from the local Larmor frequency [13]. This does not destroy the structure, however, and only leads to a smooth decrease in the size of the HPD and to an increase in the SD. As a result, the characteristic HPD lifetime is 0.1–1.0 s, much longer than the dephasing time of non-interacting spins. To summarize, a two-domain structure leads to an anomalously long-lived induction signal (LLIS). During the relaxation process the interdomain wall moves toward lower Larmor frequencies, therefore the frequency of the LLIS must fall off smoothly to  $\omega = \omega_L(z_2)$ .

#### 4. A homogeneously precessing domain under pulsed NMR conditions (experiment)

The existence of LLIS in  $^3\text{He-B}$  was first observed in Refs [14, 15], but the use of non-closed cells and the small amplitude of the LLIS made these experiments difficult to interpret. In our work [16, 17], virtually closed cells were used. The observed LLISs had large amplitudes and their frequencies were varied with time in a good agreement with the model in Section 3. Figure 3 is a schematic of the cell we used to directly prove the existence of an HPD. We placed a sample of  $^3\text{He-B}$  in a cylinder aligned along the external magnetic field and used special gradient coils to apply a controlled magnetic field

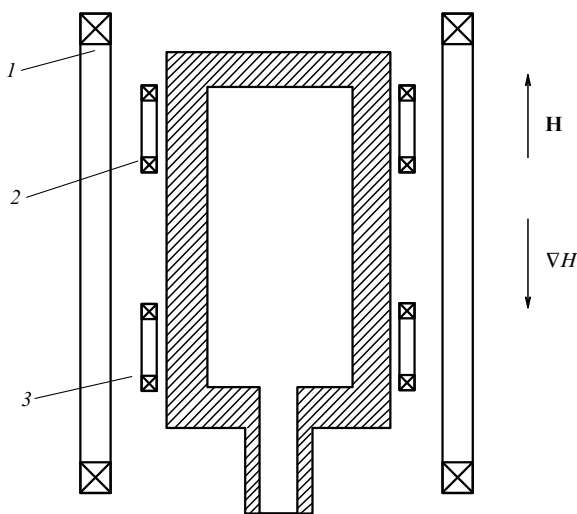


**Figure 3.** Experimental cell for HPD studies. The experimental volume is 4 mm in diameter and 8 mm in length. All the cells used were made from Stycast-1266 epoxy resin.

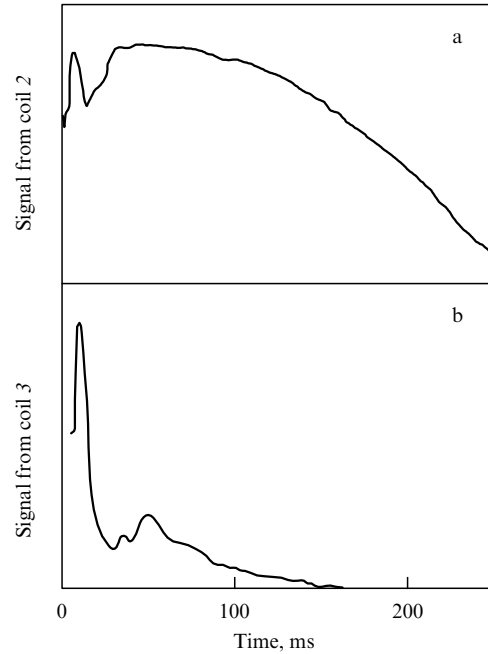


**Figure 4.** Time dependence of induction signal amplitudes from coil 2 (a) and coil 3 (b). Magnetic field and field gradient directions are as in Fig. 3.  $P = 29.3$  bar,  $H_0 = 142$  Oe,  $\nabla H = 0.1$  Oe  $\text{cm}^{-1}$ ,  $T = 0.63T_c$  (where  $T_c = 2.43$  mK is the superfluid transition temperature at 29.3 bar).

gradient to the sample. The magnetization was excited into free precession by applying a resonant rf pulse to the exciting NMR coil 1 (see Fig. 3). The induction signal was detected by two miniature pickup coils 2 and 3 located close to the opposite ends of the experimental volume; the sensitivity ranges of the coils did not overlap. Figure 4 exemplifies the time dependences of the induction signal amplitude recorded from both coils for the magnetic field gradient directed as in Fig. 3. The difference in the signals from coils 2 and 3 is explained as follows. Following the application of the rf pulse it takes about 10 ms for the two-domain structure to form. Because the static domain does not precess, the signal from coil 3 rapidly disappears (this coil is located in the large-field region, which is exactly where the SD forms); the HPD forms in the sensitivity region of coil 2, and the signal from this coil is large in amplitude. Magnetic relaxation leads to a decrease in the HPD size, therefore the amplitude of the signal from coil 2 slowly decreases, the rate of the decrease markedly increasing when the interdomain wall enters the sensitivity region of coil 2. It should be noted that the duration of the signal shown in Fig. 4a greatly exceeds the characteristic dephasing time for non-interacting spins ( $T_2^* \sim 0.7$  ms for the conditions of the experiment).

Predictably, reversing the direction of the field gradient interchanges the roles of the coils: now it is the signal from coil 2 which is found to quickly disappear, whereas that from coil 3 has a large amplitude and is observed to persist for a long time. It turned out that the magnetic relaxation of the two-domain structure also well explains the way in which the frequency of the observed LLIS depends on time. That the magnetization deviation angle in the observed HPD is close to  $\theta_0$  was checked by comparing the initial signal amplitude (Fig. 4a) with the initial amplitude of the induction signal in an identical experiment with a normal phase (where the signals from both miniature coils were practically the same and did not depend on the field gradient direction). Addi-

tional experiments confirmed that the magnetization deviation angle in the SD is zero and that it is this fact — rather than spin dephasing in the sensitivity region of coil 3 — which accounts for there being no induction signal in the case of Fig. 4b. The experiment was essentially as follows. During the existence of the HPD, a weak probe pulse was applied to that of the miniature coils in which there was no signal, and then the initial amplitude of the induction signal was compared with that of the signal the same pulse produced when applied to the unperturbed normal phase of  $^3\text{He}$ .

### 5. A homogeneously precessing domain under the conditions of continuous wave NMR

The Zeeman energy dissipated in a two-domain structure can be compensated by continuously pumping energy from a transverse, circularly polarized, small-amplitude rf field. In a coordinate system rotating at the frequency of the ( $x$ -directed) rf field, the power transfer from the rf field to the nuclear spin system of the HPD is given by

$$W = \int_V h\omega M_y dV = \int_V h\omega |\mathbf{M}| \cos\beta \sin(\alpha - \phi) dV, \quad (10)$$

where  $h$  and  $\phi$  are the amplitude and phase of the rf field, respectively. If the amplitude  $h$  is sufficiently large, the HPD precession phase  $\alpha$  can tune itself to the phase of the rf field in such a way that the power absorbed from the rf field will be equal to that dissipated in the HPD. Then, changing the rf field frequency will correspondingly change the HPD precession frequency and the interdomain wall position, the latter of which is determined, as before, by the condition that the precession frequency be equal to the local Larmor frequency. Experiments showed that an rf field of large enough amplitude ( $\sim 0.01$  Oe) makes it possible not only to maintain (and to control the length of) an already existing HPD but also to form the HPD [18]. In practice, it is more convenient to vary  $H_0$ , the spatially uniform component of the external magnetic field  $H(z) = H_0 - z\nabla H$ , than the rf field frequency.

Figure 5 shows the signals of absorption ( $\propto \int M_y dV$ ) and dispersion ( $\propto \int M_x dV$ ) obtained in such an experiment. The cell used was different from that in Fig. 3 both in size (6 mm in both diameter and length) and in having only one receiver-transmitter coil (which covered the entire experimental volume). As  $H_0$  decreases, an HPD forms at  $H_0 = H_1$  [the rf field frequency being  $gH(z_2)$ ], and the formation of the interdomain wall and its associated magnetic relaxation due to spin diffusion lead to a rapid increase in absorption. As  $H_0$  decreases still further, the area of the wall remains unchanged and the dissipation does not really increase. There is a (linear) increase in the volume of the HPD, however, which leads to the linear growth of the dispersion signal. At the field value  $H_0 = H_2$  the HPD fills the cell completely, and the domain wall disappears (more precisely, its area greatly decreases due to the HPD entering a narrow channel). As a result, the spin diffusion contribution to the magnetic dissipation is drastically reduced, the absorption drops, and the dispersion ceases to grow. Upon further decrease in  $H_0$ , the absorption resumes increasing because in the HPD the frequency shift from the local Larmor frequency increases and, accordingly, the Leggett–Takagi relaxation increases in both magnitude and importance. To compensate for this increase in absorption, the precession phase starts changing significantly. The power absorbed from the field reaches a maximum at  $\alpha - \phi = \pi/2$ ,

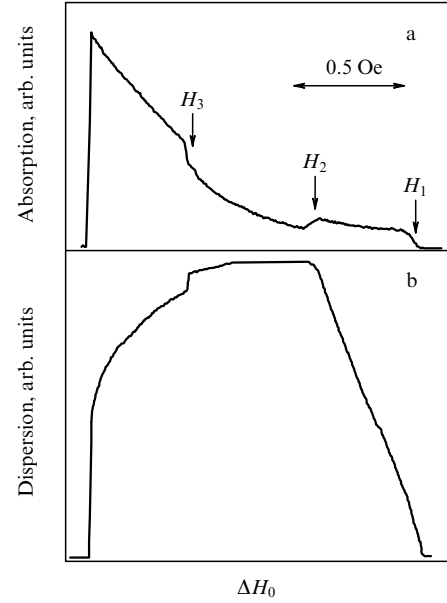


**Figure 5.** Absorption (a) and dispersions (b) signals for an HPD formed by the continuous wave NMR technique. The magnetic field gradient was directed such that the HPD formed near the upper edge of the cell and filled the entire experimental volume as  $H_0$  decreased.  $P = 11$  bar,  $H_0 = 142$  Oe,  $\nabla H = 0.83$  Oe  $\text{cm}^{-1}$ ,  $T = 0.57T_c$ .

after which the HPD is destroyed. Note that prior to this destruction, jumps of yet unknown nature are observed in the signals at  $H_0 = H_3$ . When the field is backscanned after the destruction of the HPD, the two-domain structure does not form, but there are near-standard signals with much smaller amplitudes compared to signals from the HPD. If the scanning of the field is stopped and the continuous rf field turned off before the destruction of the HPD, then an LLIS is observed, as expected.

From expression (10) it follows that when the HPD size (or equivalently, the magnetic dissipation) is held fixed, an increase in  $h$  should lead to a decrease in  $\alpha - \phi$ . In practice, already at  $h \gtrsim 0.01$  Oe the difference  $\alpha - \phi \ll \alpha$ , i.e., the rf field and the precession are practically in phase. This provides the ability to control the HPD precession phase, which proved to be very useful in experiments to study the flow of spin supercurrent through a channel.

### 6. Flow of spin supercurrent through a channel

The experimental chambers that were used in Refs [19–21] to study the flow of spin supercurrent through a channel consisted of two cells connected by a horizontal channel. Figure 6 shows what the most often used chamber looks like. In both cells, continuous rf fields created by independent receiver-transmitter NMR coils (1 and 2 in Fig. 6) helped maintain the HPDs. The point to note here is that these HPDs also ‘leaked’ into the channel, a process which was controlled using miniature pickup coils 3 and 4 on the channel. By varying the rf field phases, a difference in precession phases was created between two HPDs, with rf field amplitudes being large enough to consider that  $\Delta\alpha \approx \Delta\phi$ . The phase comparison of the signals from coils 3 and 4 revealed that a precession phase gradient developed in the channel. This led to a spin supercurrent in the channel, which transferred the longitudinal magnetization (and hence the Zeeman energy) from one HPD to another. As a result, the rf powers absorbed by the domains changed as compared to the no-spin-current

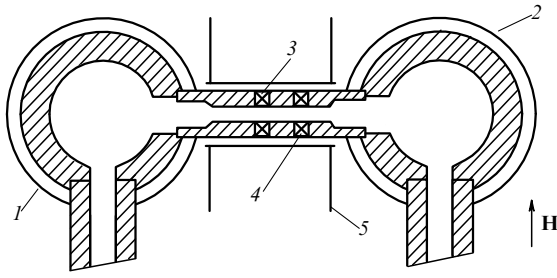


**Figure 6.** Experimental cell for superfluid spin current studies. The cell consists of two experimental volumes connected by a channel. Both volumes have the form of a cylinder (4.5 mm in diameter and 5 mm in length), whose axis lies in the horizontal plane. The narrow portion of the channel has a diameter of 0.6 mm and a length of 5.5 mm. 1 and 2 are independent receiver-transmitter rf coils, 3 and 4 are miniature pickup coils on the channel, 5 is a copper screen for screening the rf field from coils 1 and 2 in the channel region.

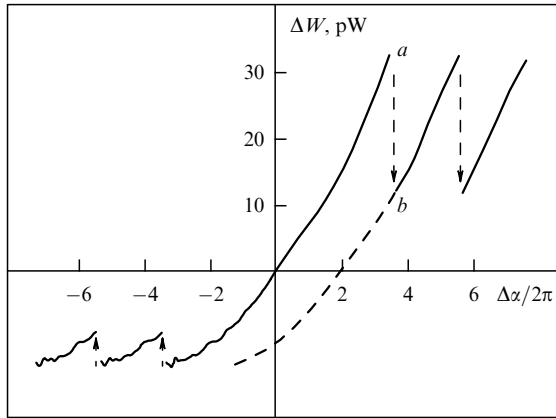


**Figure 7.** Absorption in one of the HPDs as a function of the precession phase difference between the precessing domains [left (right):  $\Delta\alpha$  decreases (increases) from  $\Delta\alpha = 0$ ]. Phase drops are shown by arrows ( $a \rightarrow b$ ). If one ceases to increase and starts decreasing the phase difference at point  $b$ , the dashed dependence and, later, the phase drops, are obtained.  $P = 29.3$  bar,  $H_0 = 142$  Oe,  $T = 0.48T_c$ .

situation: in one of the HPDs the absorption signal decreased, and in the other it increased. By measuring the change in absorption it was possible to determine the current of magnetization. It was found that as the difference in precession phases between the HPDs increased, the current increased to a certain critical value beyond which both the phase gradient and current in the channel exhibited an abrupt drop, and then the above processes repeated themselves in cycles in such a way that the period in the current– $\Delta\alpha$  dependence was always a multiple of  $2\pi$  (Fig. 7). This is due to the phase slip phenomenon and analogous to the so-called resistive state in superconducting wires. What enables the phase drop to occur is the appearance in the channel of a phase slip center with  $\beta = 0$ , which makes the phase  $\alpha$  indefinite. The magnitude of the critical spin current was obtained theoretically in Ref. [22]. According to theory, the critical value of the spin current is reached when the precession phase gradient is  $1/\xi_s$ , where the spin correlation length  $\xi_s$  is the analog of the Ginzburg–Landau correlation length of superconductivity theory. The spin correlation length depends on the difference between the HPD precession frequency  $\omega$  and the local Larmor frequency  $\omega_L$  in the

channel,

$$\xi_s = \frac{c}{\sqrt{\omega - \omega_L}}. \quad (11)$$

Thus, by varying  $H_0$  (and thereby the local Larmor frequency in the channel), it is possible to vary  $\xi_s$  in the course of the experiment (the critical current in such an experiment must be proportional to  $\sqrt{\omega - \omega_L}$ ). Note that the dependence of the current on  $\Delta\alpha$  as shown in Fig. 7 is not antisymmetric: the current flowing into the channel is always larger than the current out. The reason is that part of the transferred Zeeman energy serves to compensate the magnetic dissipation in the channel (where the rf field is zero) — with the result that the precession phase gradient varies monotonically along the channel. However, because what is measured experimentally is  $\Delta\alpha$ , not  $\alpha$ , it follows that the measured dependence of the critical current on  $\sqrt{\omega - \omega_L}$  should be compared with theoretical estimates that take into account corrections for the magnetic relaxation in the channel. Such a comparison has been made and a good agreement between theory and experiment was found in Ref. [21].

Under realistic experimental conditions, spin correlation length can reach values on the order of 1 mm. Analogy with superconductivity suggests that a sufficiently narrow and short (or a bottlenecked) channel may produce a nonhysteretic current–phase dependence, thus enabling a transition to a Josephson-like regime as found in microscopic (or tunneling) superconducting junctions. Testing this assumption involved using a cell which, unlike that of Fig. 6, had a channel bottleneck 0.3 mm in length and 0.5 mm in diameter. The experiment did reveal a nonhysteretic current–phase dependence [23]. Furthermore, because  $\xi_s$  could be varied easily in the course of the experiment, the transition from the Josephson regime to the phase slip regime was observed to occur (at  $\xi_s \sim 1$  mm as expected).

The fact that magnetic relaxation violates spin conservation does not run counter to the notion of nondissipative spin supercurrent, which is caused by order parameter phase gradients rather than the difference in pressure or chemical potential. Dissipation leading to the nonconservation of channel current is not due directly to the current but to the non-spin-conserving magnetic relaxation. Spin current in the experiment above is akin to the flow of superfluid  $^3\text{He}$  which evaporates as it flows in a heated open trough. In this case, the current flowing out of the trough is also less than that flowing into it, and it is the violation of conservation of mass due to evaporation which serves as the analog of magnetic dissipation.

## 7. Research applications of the HPD

The follow-up research involved the magnetic analogs of phenomena found in ‘usual’ superfluid systems. One result in this area was the creation and observation of the spin vortex, a magnetic analog of the quantum vortex [24, 25]. Observations were also made of various modes of the spatially nonuniform HPD vibrations, [26] one of which (the so-called twisting mode) is the analog of the fourth sound in  $^4\text{He}$ . One useful application of the HPD is in the study of the properties of superfluid  $^3\text{He-B}$ . In particular, the interaction of HPDs with quantum vortices in  $^3\text{He-B}$  [27, 28] and with the counterflow of the normal and superfluid components [29] was studied using the rotating cryostat at the Helsinki University of Technology, Finland — experiments which

resulted in confidently identifying vortices of different types in measurements of the magnetic-field-induced superfluid density anisotropy in  $^3\text{He-B}$ . A study of the relaxation of HPDs enabled a systematic measurement of magnetic relaxation parameters [30]. With its property of a spatially uniform order parameter distribution (texture), the homogeneously precessing domain can be effective in studying texture-sensitive phenomena. In particular, the use of the HPD has permitted Leggett frequency measurements in the B-like  $^3\text{He}$  phase in an aerogel, whose effect on the texture makes standard NMR methods difficult to use for this purpose [31].

## 8. Conclusion

In summary, the studies reviewed prove the existence of spin supercurrents in  $^3\text{He-B}$  and demonstrate the analogy between spin superfluidity on the one hand and ‘usual’ mass superfluidity and superconductivity on the other. As a result, many experiments were explained and new research directions identified. For example, the electric field should play the same role for spin supercurrent that the magnetic field vector-potential does for superconducting electrons. Although very small in magnitude, this effect can in principle be measured. Also of interest might be to conduct research at ultralow temperatures of around 100  $\mu\text{K}$ , where, even though spin supercurrents are clearly important, very long (of the order of an hour) induction signals are observed which the HPD formation model fails to describe [32]. The homogeneously precessing domain was observed not only in  $^3\text{He-B}$  but also in the B-like phase of  $^3\text{He}$  in an aerogel — which, in particular, supports interpreting this phase as the analog of the B-phase of the ‘usual’ bulk  $^3\text{He}$  as well as opens new possibilities for its study [33].

Dissipationless (reactive) spin currents can exist in other magnetic systems. At sufficiently low temperatures and high magnetic fields, the effective spin diffusion coefficient in Fermi liquids becomes complex, allowing for dissipationless spin currents [34] and thereby leading to a number of phenomena, some of which are analogous to those observed in  $^3\text{He-B}$  [35, 36]. For example, normal liquid  $^3\text{He}$  and  $^3\text{He-}^4\text{He}$  solutions were observed to exhibit a structure of two oppositely magnetized domains with an in-phase precessing domain wall [37, 38]. In principle, similar phenomena can also occur in magnetically ordered solids. This requires, in addition to the small magnetic relaxation, that the order parameter be degenerate with respect to one of its orientation angles and that the corresponding gradient term be present in the Hamiltonian. Magnetically ordered solid  $^3\text{He}$  [39] and antiferromagnet  $\text{CsNiCl}_3$  [40] are candidate materials for such studies.

## References

1. Vollhardt D, Wölfle P *The Superfluid Phases of  $^3\text{He}$*  (London: Taylor & Francis, 1990)
2. Mineev V P *Usp. Fiz. Nauk* **139** 303 (1983) [*Sov. Phys. Usp.* **26** 160 (1983)]
3. Abragam A, Goldman M *Nuclear Magnetism: Order and Disorder* (Oxford: Clarendon Press, 1982) [Translated into Russian (Moscow: Mir, 1984)]
4. Osheroff D D et al. *Phys. Rev. Lett.* **29** 920 (1972)
5. Borovik-Romanov A S, Bunkov Yu M *Sov. Sci. Rev. Sec. A Phys.* **15** 1 (1990)
6. Fomin I A, in *Helium Three* (Modern Problems in Condensed Matter Sciences, Vol. 26, Eds W P Halperin, L P Pitaevskii) (Amsterdam: North-Holland, 1990) p. 609

7. Bunkov Yu M, in *Progress in Low Temperature Physics* Vol. 14 (Ed. W P Halperin) (Amsterdam: Elsevier Sci. Publ., 1995) p. 69
8. Dmitriev V V, Fomin I A *J. Low Temp. Phys.* **135** 361 (2004)
9. Leggett A J *Ann. Phys. (New York)* **85** 11 (1974)
10. Leggett A J, Takagi S *Ann. Phys. (New York)* **106** 79 (1977)
11. Brinkman W F, Smith H *Phys. Lett. A* **53** 43 (1975); Osheroff D D, Corruccini L R, in *Proc. of the 14th Intern. Conf. on Low Temperature Physics, LT-14* Vol. 1 (Eds M Krusius, M Vuorio) (Amsterdam: North-Holland, 1975) p. 100
12. Fomin I A *Zh. Eksp. Teor. Fiz.* **93** 2002 (1987) [*Sov. Phys. JETP* **66** 1142 (1987)]
13. Fomin I A *Pis'ma Zh. Eksp. Teor. Fiz.* **40** 260 (1984) [*JETP Lett.* **40** 1037 (1984)]; *Zh. Eksp. Teor. Fiz.* **88** 2039 (1985) [*Sov. Phys. JETP* **61** 1207 (1985)]
14. Corruccini L R, Osheroff D D *Phys. Rev. B* **17** 126 (1978)
15. Giannetta R W, Smith E N, Lee D M J. *Low Temp. Phys.* **45** 295 (1981)
16. Borovik-Romanov A S et al. *Pis'ma Zh. Eksp. Teor. Fiz.* **40** 256 (1984) [*JETP Lett.* **40** 1033 (1984)]
17. Borovik-Romanov A S et al. *Zh. Eksp. Teor. Fiz.* **88** 2025 (1985) [*Sov. Phys. JETP* **61** 1199 (1985)]
18. Borovik-Romanov A S et al. *Zh. Eksp. Teor. Fiz.* **96** 956 (1989) [*Sov. Phys. JETP* **69** 542 (1989)]
19. Borovik-Romanov A S et al. *Pis'ma Zh. Eksp. Teor. Fiz.* **45** 98 (1987) [*JETP Lett.* **45** 124 (1987)]
20. Borovik-Romanov A S et al. *Jpn. J. Appl. Phys.* **26** 175 (1987)
21. Borovik-Romanov A S et al. *Phys. Rev. Lett.* **62** 1631 (1989)
22. Fomin I A *Pis'ma Zh. Eksp. Teor. Fiz.* **45** 106 (1987) [*JETP Lett.* **45** 135 (1987)]
23. Borovik-Romanov A S et al. *Pis'ma Zh. Eksp. Teor. Fiz.* **47** 400 (1988) [*JETP Lett.* **47** 478 (1988)]
24. Fomin I A *Zh. Eksp. Teor. Fiz.* **94** (11) 112 (1988) [*Sov. Phys. JETP* **67** 1148 (1988)]
25. Borovik-Romanov A S et al. *Physica B* **165–166** 649 (1990)
26. Bunkov Yu M, Dmitriev V V, Mukharskii Yu M *Physica B* **178** 196 (1992)
27. Bunkov Yu M, Hakonen P J J. *Low Temp. Phys.* **83** 323 (1991)
28. Kondo Y et al. *Phys. Rev. Lett.* **67** 81 (1991)
29. Korhonen J S et al. *Phys. Rev. B* **46** 13983 (1992)
30. Bunkov Yu M et al. *Phys. Rev. Lett.* **65** 867 (1990)
31. Dmitriev V V et al. *Pis'ma Zh. Eksp. Teor. Fiz.* **79** 612 (2004) [*JETP Lett.* **79** 499 (2004)]
32. Bunkov Yu M et al. *Phys. Rev. Lett.* **69** 3092 (1992)
33. Dmitriev V V et al. *Pis'ma Zh. Eksp. Teor. Fiz.* **76** 371 (2002) [*JETP Lett.* **76** 312 (2002)]
34. Leggett A J, Rice M J *Phys. Rev. Lett.* **20** 586 (1968); Leggett A J *J. Phys. C: Solid State Phys.* **3** 448 (1970)
35. Fomin I A *Physica B* **210** 373 (1995)
36. Dmitriev V V, Fomin I A *Pis'ma Zh. Eksp. Teor. Fiz.* **59** 352 (1994) [*JETP Lett.* **59** 378 (1994)]
37. Dmitriev V V, Zakazov S R, Moroz V V *Pis'ma Zh. Eksp. Teor. Fiz.* **61** 309 (1995) [*JETP Lett.* **61** 324 (1995)]; Dmitriev V V, Moroz V V, Zakazov S R *J. Low Temp. Phys.* **101** 141 (1995)
38. Dmitriev V V et al. *Physica B* **210** 366 (1995)
39. Fomin I A, Shopova D V *Pis'ma Zh. Eksp. Teor. Fiz.* **42** 162 (1985) [*JETP Lett.* **42** 199 (1985)]
40. Mineev V P *Zh. Eksp. Teor. Fiz.* **110** 2211 (1996) [*JETP* **83** 1217 (1996)]

PACS numbers: **75.10. - b**, **75.25. + z**, 75.50.Ee  
DOI: 10.1070/PU2005v048n01ABEH002112

## New magnetic states in crystals

S S Sosin, L A Prozorova, A I Smirnov

### 1. Introduction

One of the major types of magnetic interactions in crystals is the exchange interaction, which is usually described by a